

Rate Dependence of Elementary Rearrangements and Spatiotemporal Correlations in the 3D Flow of Soft Solids

Vishwas V. Vasisht, Sudeep K. Dutta, Emanuela Del Gado, and Daniel L. Blair
*Department of Physics, Institute for Soft Matter Synthesis and Metrology, Georgetown University,
 37th and O Streets, N.W., Washington, DC 20057, USA*

 (Received 8 June 2017; published 5 January 2018)

We use a combination of confocal microscopy, rheology, and molecular dynamics simulations to investigate jammed emulsions under shear, by analyzing the 3D droplets rearrangements in the shear frame. Our quantitative analysis of local dynamics reveals elementary nonaffine rearrangements that underlie the onset of the flow at small strains. We find that the mechanism of unjamming and the upturn in the material flow curve are associated to a qualitative change in spatiotemporal correlations of such rearrangements with the applied shear rate. At high shear rates, droplet clusters follow coordinated, stringlike motion. Conversely, at low shear rates, the elementary nonaffine rearrangements exhibit longer-ranged correlations, with complex spatiotemporal patterns. The 3D microscopic details provide novel insights into the specific features of the material flow curve, common to a large class of technologically relevant soft disordered solids and new fundamental ingredients for constitutive models.

DOI: [10.1103/PhysRevLett.120.018001](https://doi.org/10.1103/PhysRevLett.120.018001)

Emulsions are widely used in a variety of industrial processes; applications are found in the formation or transport of value-added materials, including foods, pharmaceuticals, and personal care products [1]. When highly concentrated emulsions become soft solids and exhibit rheological behavior, that depends strongly on the shear rate, similar to many other jammed soft solids [2–7]. The empirical Herschel-Bulkley (HB) relation describes the macroscopic flow curve that relates the steady state shear stress σ to the shear rate $\dot{\gamma}$ as $\sigma = \sigma_Y + K\dot{\gamma}^n$, where σ_Y is the yield stress and K and n are material specific constants. For $n \sim 0.5$, the curve can be understood in terms of a nonlocal constitutive relationship [8,9], which assumes that close to yielding, plastic and irreversible rearrangements determine the local mechanism for shear stress dissipation [3,10–14]. Mean-field theories that describe the yielding process in soft solids invoke avalanchelike plastic rearrangements that occur within a nearly continuum elastic background at infinitesimal rates [14–17]. Numerical simulations of flowing jammed solids provide additional insights to the connection between bulk flow and microscopic deformations [18–21]. What remains unclear is a fully three-dimensional picture that includes the development of spatial correlations of the elementary microscopic rearrangements (EMR), in particular, as a function of the shear rate. Understanding the role of the deformation rate in a wide range of soft solids is crucial to most technological applications. In yielding foams [7,22], where the EMR are typically classified as “T1-events,” spectroscopy indicates that correlations are spatially extended and strongly rate dependent, a signature also recently described in emulsions [23,24]. From a fundamental point of view, the relationship

between σ and $\dot{\gamma}$ is well understood for systems where the initial microstructure is sufficiently close to isostaticity [25,26]. However, for a wide range of soft solids, the microstructure can be overconstrained and well beyond isostaticity [27]. Thus, new insight into the rate dependent spatiotemporal correlations of EMR is needed to develop a coherent framework for the macroscale rheology. In this Letter, we combine confocal rheology experiments and numerical simulations to quantitatively describe the droplet scale rearrangements in a sheared three-dimensional compressed emulsion. Through our analysis of EMR in experiments and simulations, we find that the flow at high shear rates originates from a highly coordinated motion of small particle clusters that move collectively in the same direction. Conversely, at low shear rates, the bulk flow emerges from nonaffine rearrangements that take place over much larger correlated domains and trigger events later in time, due to the long-range elastic strain field of the initially solid amorphous material. The nature of the nonaffine rearrangements and their spatiotemporal correlations shows a clear dependence on the flow rate, and it qualitatively changes over shear rates corresponding to the upturn of the material flow curve. By elucidating fundamental microscopic mechanisms for flow that have relevance beyond the experimental system considered here, our results provide a crucial step towards developing constitutive models needed to design and control the flow of a wide range of jammed soft solids.

Experiments.—The experimental system is a direct emulsion of silicone oil droplets stabilized with the surfactant sodium dodecyl sulfate (SDS) in an index-matched continuous phase of water, glycerol, and fluorescein [see Supplemental Material (SM) [28]]. The droplets,

with an average diameter of $6.0 \mu\text{m}$ and a polydispersity of 0.15, were compressed above the jamming point with centrifugation [33]. Measurements of the system under flow were performed with a rheometer integrated with a confocal microscope [34]. The rheometer gap is formed by a plate tool and glass coverslip, providing optical access, and a parallel plate tool. Images were taken at a fixed relative position between the two instruments, where the local velocity, vorticity, and gradient axes will be referred to as x , y , and z , respectively.

We measure the influence of shear rate on the local droplet dynamics by acquiring and analyzing time-resolved fluorescence confocal images, while the rheometer simultaneously applies a continuous rotation at a fixed strain rate $\dot{\gamma}$ (see SM). For $\dot{\gamma} \leq 10^{-2} \text{ s}^{-1}$, time-resolved 3D stacks are acquired, while at higher shear rates, we acquire 2D images at z positions that are equally spaced throughout the rheometer gap. In the case of 2D imaging, where particle locating and tracking is not possible, time-resolved spatial cross correlations are calculated between pairs of consecutive images at a given z position to quantify the spatially-resolved droplet-scale velocities $v(x, y)|_z$, which are compared against particle tracking. The averaged velocities are calculated as a function of z to determine the velocity profiles at each $\dot{\gamma}$ and obtain the local shear rate $\dot{\gamma}_l$. The analysis is performed for two different volume fractions, well beyond the onset of jamming, and we present data for $\phi = 0.70$ (see SM).

The flow curves for our emulsions exhibit HB rheology, with $n \approx 0.51$ for $\phi = 0.70$ and a corresponding dependence on σ_y that increases with ϕ [see Fig. 1(a)]. After removing the local shear flow from the confocal images, we obtain a

vector displacement field, with components Δx and Δy . In Fig. 1(a), we plot the mean square displacement (MSD) $\langle \Delta r^2 \rangle = \langle \Delta x^2 + \Delta y^2 \rangle$, as a function of the accumulated strain $\Delta\gamma = \dot{\gamma}_l \Delta t$, over a wide range of applied shear rates, where $\dot{\gamma}_l$ is the local shear rate, taking into account the local velocity fluctuations in the shear frame. At the highest shear rates ($\dot{\gamma} \geq 1 \text{ s}^{-1}$), the system exhibits superdiffusive behavior at small $\Delta\gamma$, followed by a diffusive regime, whereas at lower strain rates, the $\langle \Delta r^2 \rangle$ show diffusive behavior over the entire range. The transition between these two different behaviors takes place over the shear rates at which the flow curve [Fig. 1(a)] bends, departing from the low $\dot{\gamma}$ plateau. While we use the in-plane MSD for simplicity, we note that the analysis and the data reported entail a fully 3D quantification of the EMR, since motion along the gradient direction and the coupled motion across vorticity planes with different z coordinates are included. Moreover, in our experiments, we have access to the full distribution of the droplet displacements or the self-part of the van Hove correlation function $G_S(r, \Delta\gamma)$ [35–37], in the shear frame for a chosen strain window $\Delta\gamma$, which clearly shows non-Gaussian statistics. The data for $\Delta\gamma = 0.02$ and $\Delta\gamma = 0.10$ are displayed in Figs. 1(c), 1(d) and, whereas at a large $\Delta\gamma$ the distributions exhibit exponential tails for all $\dot{\gamma}$, the data at small $\Delta\gamma$, which provide information on the EMR, clearly feature a power-law tail at low $\dot{\gamma}$. While the data at all $\Delta\gamma$ indicate that the underlying microscopic motion is far from a simple picture of shear induced diffusive motion, the data for a small $\Delta\gamma$ indicates that the distinctive features of EMR strongly depend on the imposed shear rate. The power-law tails in $G_S(r, \Delta\gamma)$ are

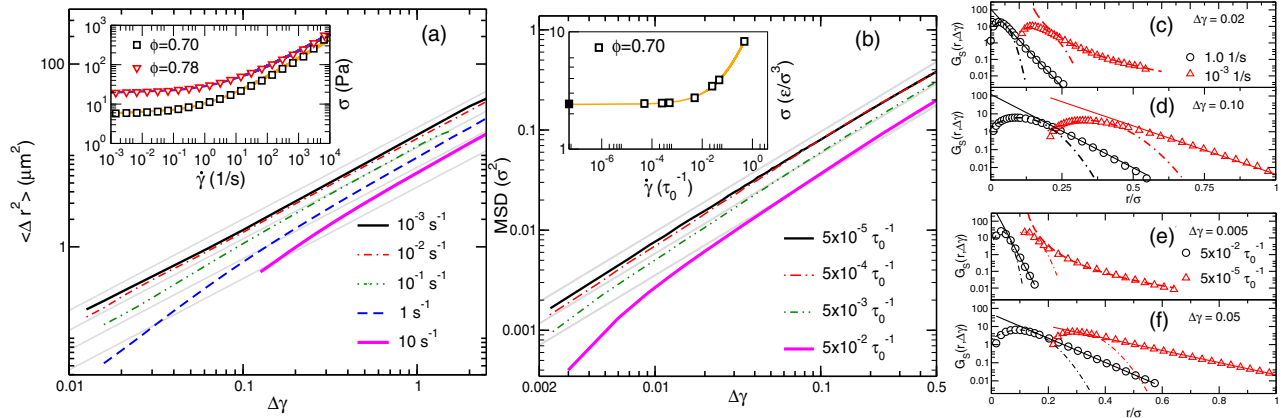


FIG. 1. (a) The shear-frame MSD ($\langle \Delta r^2 \rangle$) measured in the x, y plane at $\phi = 0.70$. The gray solid lines indicate diffusive behavior. (inset) Experimental flow curves for $\phi = 0.70$ and $\phi = 0.78$ and the solid lines represent a HB fit, with flow indices of $n = 0.51$ and $n = 0.45$. (b) The nonaffine MSD computed in the x, y plane from simulations. (inset) Simulation flow curve. The shear stress σ as a function of the shear rate $\dot{\gamma}$ measured at volume fraction $\phi = 0.70$ and the solid lines are a HB fit, with a flow index of 0.6. The solid square data obtained from the quasistatic simulations that correspond to a zero shear rate condition. The linear modulus is $G' = 180, 360 \text{ Pa}$ for $\phi = 0.70, 0.78$. The experimental van Hove correlation function $G_S(r, \Delta\gamma)$ is computed at $\phi = 0.70$ for two different strain windows, (c) $\Delta\gamma = 0.02$ and (d) $\Delta\gamma = 0.1$, for two different shear rates, 1.0 s^{-1} and 10^{-3} s^{-1} . The $G_S(r, \Delta\gamma)$ computed for (e) from simulations $\Delta\gamma = 0.005$, and (f) $\Delta\gamma = 0.005$ for shear rates $\dot{\gamma} = 5 \times 10^{-2} \tau_0^{-1}$, and $\dot{\gamma} = 5 \times 10^{-5} \tau_0^{-1}$. For the purpose of clarity we have shifted the abscissa of the distribution function by a constant factor of 0.2 for $5 \times 10^{-5} \tau_0^{-1}$. The dot-dashed line is the best fit with a Gaussian, and the solid and dashed lines correspond to the best fit with an exponential and power law, respectively.

detected consistently in the plateau regime of the flow curve, and they suggest plastic rearrangements are occurring in an elastic background; i.e., the elasticity of the initially jammed solid plays a significant role in the steady state reached at a low enough shear rate [21,38,39]. The exponential tails are reminiscent of correlated and heterogeneous dynamics in supercooled liquids and, at a small $\Delta\gamma$, they appear at shear rates for which the shear stress σ starts to deviate from the plateau [40]. This suggests a distinct change in the elementary rearrangements as a function of shear rate.

Numerical simulations.—To gain insights and broaden the scope of our experimental results, we complement the experiments with three-dimensional numerical simulations of 10% polydisperse spheres that interact through short ranged repulsion, subjected to shear deformations. We utilize the Weeks-Chandler-Anderson form of the truncated Lennard-Jones potential, defined as $U(r) = 4\epsilon[(a_{ij}/r_{ij})^{12} - (a_{ij}/r_{ij})^6] + \epsilon$, for $r_{ij} \leq 2^{1/6}a_{ij}$, else $U(r_{ij}) = 0$ [41]. Here, ϵ defines the energy unit, independent of particle diameter a , $a_{ij} = (a_i + a_j)/2$ defines the distance between the center of particles i and j at contact. While other numerical studies have focused on models more specifically designed for emulsions [4,42], our model generically describes short range soft repulsive interactions common to many soft glassy solids [43]. Hence, it has the purpose to verify that the shear rate dependence of EMR found in the experiments is not due to our specific experimental system. The numerical samples consist of 97556 particles at $\phi \sim 70\%$ in cubic simulation box of dimension $l_x = l_y = l_z = 42a$. All samples are initially prepared via Molecular Dynamics (MD) by melting a crystal at high temperature, carefully quenching it to $k_B T/\epsilon = 10^{-3}$, and subsequently bringing it to the closest energy minimum and to $k_B T/\epsilon \approx 0$ using energy minimization (see SM), to obtain an amorphous solid. We perform finite shear rate simulations that solve the equation of motion,

$$m \frac{d^2 \vec{r}_i}{dt^2} = -\zeta \left(\frac{d\vec{r}_i}{dt} - \dot{\gamma} z_i \vec{e}_x \right) - \nabla_{\vec{r}_i} U, \quad (1)$$

with Lees-Edwards boundary conditions. Here, $\dot{\gamma}$ represents the applied shear rate, m the particle mass, \vec{r}_i the position vector of the particle i , z_i the z coordinate of particle i , and \vec{e}_x the unit vector along the x axis. The damping coefficient ζ is chosen such that $m/\zeta = 2.0$, and the shear rate $\dot{\gamma}$ is expressed in the unit of τ_0^{-1} , where $\tau_0 = \zeta a^2/\epsilon$, which is the time scale associated to a particle moving under a unit force ϵ/a over a distance a and experiencing the drag ζ . Hydrodynamic interactions are not included, assuming they are screened at these high volume fractions, and the choice made for m/ζ guarantees inertial effects are minimal and the motion is effectively overdamped.

The flow curve obtained in steady state from the simulations at $\phi = 0.70$ follows the HB form with a flow

index $n \approx 0.6$ [Fig. 1(b)]. The differences in n between experiments and simulations may originate from interactions between droplets mediated by the liquid films [12,44,45] and van der Waals attractions between droplets [46]. In both systems, the initial soft solid is compressed above its jamming threshold, as indicated by the absence of the scaling behavior predicted in [26] close to the jamming transition (see SM). We note that in the simulations, the value of the shear stress σ at the lowest $\dot{\gamma}$ probed is comparable to the *quasistatic* simulations, supposedly representing the zero shear rate limit, and the plateau in σ extends over a range, which is qualitatively comparable with experiments. We analyze particle displacements and their spatiotemporal correlations at and above plateau regime. We obtain the nonaffine displacement vector field and displacement distributions (see Fig. 1) identical to our experiments. Remarkably, for conditions equivalent to those shown in Fig. 1(a), the simulations capture all of the essential features found in the experimental results. Most notably, for a small $\Delta\gamma$, the MSD obtained in the simulations exhibits a cross-over from superdiffusive to diffusive motion with increasing $\dot{\gamma}$, while the van Hove functions exhibit the same change from exponential to power law behavior with decreasing $\dot{\gamma}$ as shear stress deviates from the plateau regime in the flow curve. The similarities in these essential microscopic metrics in simulations and experiments are remarkable, especially in view of the simple model used, which only accounts for the soft glassy nature of the solid formed. Our findings support the idea that the interdependencies detected in experiments have a more general relevance to a wider range of soft solids, and this encourages us to investigate particle-level details in our simulations.

We measure the displacement correlation function S_U , defined as $S_U(\Delta r, \Delta\gamma) = \langle \vec{U}_i \cdot \vec{U}_j \rangle / \langle U^2 \rangle$, where $\vec{U} = U_x \hat{i} + U_y \hat{j}$ is the displacement vector of a droplet in the x, y plane and i and j being particle index [23,36] for the simulations. Completely correlated (anticorrelated) displacements give $S_U = 1.0$ ($S_U = -1.0$). S_U is shown in Figs. 2(a) and (b), at respectively high and low rates over different strain windows $\Delta\gamma$. In each case, we extract a correlation length ξ by fitting the data with an exponential function and averaging the fit parameters over the z direction. The correlation lengths ξ are shown in Fig. 2(c) as a function of the $\Delta\gamma$, indicating striking differences between high and low rates. The range of spatial correlation of displacements at high rates is nearly constant at $\xi \sim 2-5a$ for all values of $\Delta\gamma$, whereas at the low shear rates, $\xi \approx 15a$ for small strain intervals, decreasing dramatically as $\Delta\gamma$ is increased. At the lowest rates, the value of ξ for small $\Delta\gamma$ is limited only by the system size, since $S_U(r)$ features a slower power law decay following the initial exponential decay [see Fig. 2(a)]. ξ provides an estimate of the typical size of an EMR, indicating a significant shear rate dependence. $S_U(\Delta r, \Delta\gamma)$ can be decomposed into longitudinal S_U^L and transverse S_U^T components [36], whose ratio obtained at

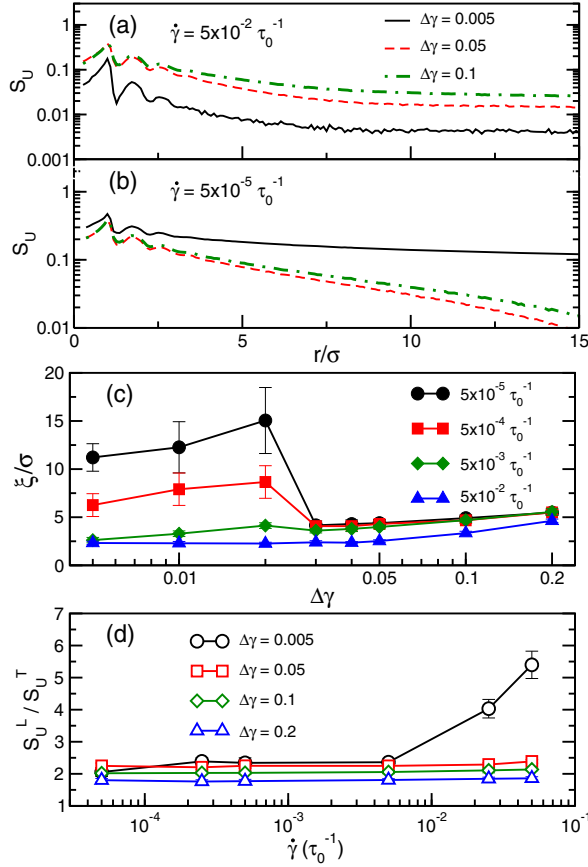


FIG. 2. (a) S_U at a high shear rate $\dot{\gamma} = 5 \times 10^{-2} \tau_0^{-1}$, and a low shear rate (b) $\dot{\gamma} = 5 \times 10^{-5} \tau_0^{-1}$. (c) the correlation length from S_U as a function shear strain, for all shear rates. (d) the ratio of longitudinal to transverse displacement correlation function measured at a distance of 1σ .

$\Delta r \approx 1.0a$ is plotted in Fig. 2(d) as a function of $\dot{\gamma}$. For the rates and strain windows corresponding to the superdiffusive regime of the MSD where $\dot{\gamma} < 10^{-2} \tau_0^{-1}$ and $\Delta\gamma < 10^{-2}$ [see Fig. 2(c)], the dominant contribution to the spatial correlations of the EMR comes from S_U^L , indicating that EMR are coordinated *stringlike* groups of particles reminiscent of dynamical heterogeneities in supercooled liquids [47] (see SM Movies M3–M8). In contrast, for rates within the stress plateau, an EMR can involve a significant fraction of the particles in a far less directional motion. The large error bars in the correlation length at low rates are due to fluctuations in the instantaneous velocity profiles, revealing a flow behavior that is both inhomogeneous and intermittent. Nonaffine displacement maps obtained at fixed shear rates qualitatively support our conclusions. Representative maps for experiments and simulations are shown in Fig. 3. At a high $\dot{\gamma}$, we observe relatively small displacements that are partially homogeneous [see Figs. 3(a),(b)], while at lower values, the displacements become highly localized, *bursty*, and heterogeneous [see Figs. 3(c),(d); Movies M1 and M2 in the SM], consistent with the predictions of elastoplastic models for amorphous solids [21,38,39].

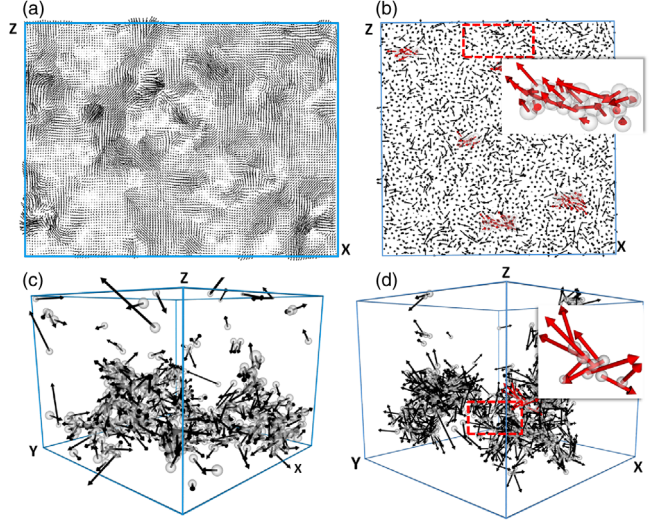


FIG. 3. Nonaffine displacement maps from experiments computed at (a) ($\dot{\gamma} = 1.0 \text{ s}^{-1}$, $\Delta\gamma \approx 0.015$) and (c) ($\dot{\gamma} = 3 \times 10^{-3} \text{ s}^{-1}$, $\Delta\gamma \approx 0.05$). The rendered particle positions are approximately taken from the middle third of the rheometer gap. Similar maps from simulations for (b) $\dot{\gamma} = 5 \times 10^{-2} \tau_0^{-1}$ and (d) $\dot{\gamma} = 5 \times 10^{-5} \tau_0^{-1}$, at $\langle \Delta\gamma \rangle \approx 0.005$. The arrows represent the nonaffine displacement vector. To highlight the localization of displacement vectors, the length of the vectors are amplified. For clarity and comparison, we show only a 2D plane for simulations (see SM for 3D images and movies). Images rendered using [48].

Conclusions.—Our results provide microscopic insights into the nonequilibrium flow properties of soft solids by connecting the 3D microscopic dynamics to the macroscopic flow behavior. We show that the 3D particle scale rearrangements and spatiotemporal correlations are intrinsically coupled to the imposed shear rate. The steady-state response of unjammed emulsions, defined by the bulk rheological flow curve of the material, is closely associated with changes in the nature of the EMR that are governed by the onset of microscopic flow. When the flow is parametrized by the local accumulated strain, two distinct and rate dependent microscopic mechanisms are observed as the signatures of stress relaxation and yielding. Directionally correlated, stringlike motion is found in the flowing state well above the yield stress. In contrast, near the yield stress, the primary mechanism for stress relaxation is localized plastic bursts embedded within an elastic continuum. These bursts exhibit long range spatiotemporal correlations and are strongly reminiscent of the local elastically interacting rearrangements that underlie plasticity in amorphous solids, referred to as shear transformations [3,49,50]. The picture of yielding and flow in jammed soft solids that we obtain is consistent with previous experimental findings in foams using diffusive wave spectroscopy [7], while adding insights to its physical interpretation and extending it to a wider range of materials. The quantitative analysis of the spatiotemporal correlations of the EMR indicate that the correlation range and intensity

change qualitatively with the rate. The two results together suggest that the change in the spatiotemporal correlations may be at the origin of, or must be coupled to, the differences in the flow events when the material is sheared at different rates. Moreover, the differences and dependence of the microscopic nonaffine dynamics with the imposed shear rate are an essential components of the nonlinear dependence on the rate of the flow curve; suggesting that the qualitative change in the spatiotemporal correlation pattern of the nonaffine particle motion determines the upturn in the flow curve, common to a wide range of soft materials. Recognizing the distinct and rate dependent nature of the elementary excitations in jammed soft materials a fundamental starting point for the development of microscopic theories and constitutive models [5,51–53].

-
- [1] J. Bibette, F. Leal-Calderon, V. Schmitt, and P. Poulin, *Emulsion Science: Basic Principles. An Overview*, Springer Tracts in Modern Physics (Springer-Berlin, Heidelberg, 2003).
- [2] J.-R. Huang and T. G. Mason, *Soft Matter* **5**, 2208 (2009).
- [3] P. Schall, D. A. Weitz, and F. Spaepen, *Science* **318**, 1895 (2007).
- [4] J. R. Seth, L. Mohan, C. Locatelli-Champagne, M. Cloitre, and R. T. Bonnecaze, *Nat. Mater.* **10**, 838 (2011).
- [5] J. Goyon, A. Colin, G. Ovarlez, A. Ajdari, and L. Bocquet, *Nature (London)* **454**, 84 (2008).
- [6] T. Divoux, D. Tamarii, C. Barentin, and S. Manneville, *Phys. Rev. Lett.* **104**, 208301 (2010).
- [7] A. Gopal and D. Durian, *J. Colloid Interface Sci.* **213**, 169 (1999).
- [8] P. Hébraud and F. Lequeux, *Phys. Rev. Lett.* **81**, 2934 (1998).
- [9] A. Nicolas, K. Martens, L. Bocquet, and J.-L. Barrat, *Soft Matter* **10**, 4648 (2014).
- [10] A. Argon, *Acta Metall.* **27**, 47 (1979).
- [11] M. L. Falk, *Science* **318**, 1880 (2007).
- [12] N. D. Denkov, S. Tcholakova, K. Golemanov, K. P. Ananthapadmanabhan, and A. Lips, *Phys. Rev. Lett.* **100**, 138301 (2008).
- [13] K. E. Jensen, D. A. Weitz, and F. Spaepen, *Phys. Rev. E* **90**, 042305 (2014).
- [14] J. Lin and M. Wyart, *Phys. Rev. X* **6**, 011005 (2016).
- [15] C. Heussinger, L. Berthier, and J.-L. Barrat, *Europhys. Lett.* **90**, 20005 (2010).
- [16] C. Heussinger, P. Chaudhuri, and J.-L. Barrat, *Soft Matter* **6**, 3050 (2010).
- [17] K. Martens, L. Bocquet, and J.-L. Barrat, *Phys. Rev. Lett.* **106**, 156001 (2011).
- [18] M. Talamali, V. Petäjä, D. Vandembroucq, and S. Roux, *Phys. Rev. E* **84**, 016115 (2011).
- [19] C. E. Maloney and A. Lemaître, *Phys. Rev. E* **74**, 016118 (2006).
- [20] C. E. Maloney and M. O. Robbins, *J. Phys. Condens. Matter* **20**, 244128 (2008).
- [21] A. Lemaître and C. Caroli, *Phys. Rev. Lett.* **103**, 065501 (2009).
- [22] D. Chen, D. Semwogerere, J. Sato, V. Breedveld, and E. R. Weeks, *Phys. Rev. E* **81**, 011403 (2010).
- [23] E. D. Knowlton, D. J. Pine, and L. Cipelletti, *Soft Matter* **10**, 6931 (2014).
- [24] K. W. Desmond and E. R. Weeks, *Phys. Rev. Lett.* **115**, 098302 (2015).
- [25] P. Olsson and S. Teitel, *Phys. Rev. Lett.* **99**, 178001 (2007).
- [26] B. P. Tighe, E. Woldhuis, J. J. C. Remmers, W. van Saarloos, and M. van Hecke, *Phys. Rev. Lett.* **105**, 088303 (2010).
- [27] T. Lubensky, C. Kane, X. Mao, A. Souslov, and K. Sun, *Rep. Prog. Phys.* **78**, 073901 (2015).
- [28] See Supplemental Material at <http://link.aps.org/supplemental/10.1103/PhysRevLett.120.018001> for additional information and movies about the experimental and simulation results. The Supplemental Material also includes Refs. [29–32].
- [29] J. Brujić, S. F. Edwards, D. V. Grinev, I. Hopkinson, D. Brujić, and H. A. Makse, *Faraday Discuss. Chem. Soc.* **123**, 207 (2003).
- [30] J. C. Crocker and D. G. Grier, *J. Colloid Interface Sci.* **179**, 298 (1996).
- [31] P. J. Steinhardt, D. R. Nelson, and M. Ronchetti, *Phys. Rev. B* **28**, 784 (1983).
- [32] A. Rahman, *Phys. Rev.* **136**, A405 (1964).
- [33] J. Bibette, *J. Colloid Interface Sci.* **147**, 474 (1991).
- [34] S. K. Dutta, A. Mbi, R. C. Arevalo, and D. L. Blair, *Rev. Sci. Instrum.* **84**, 063702 (2013).
- [35] J.-P. Hansen and I. R. McDonald, *Theory of Simple Liquids* (Elsevier, New York, 1990).
- [36] E. R. Weeks, J. C. Crocker, and D. A. Weitz, *J. Phys. Condens. Matter* **19**, 205131 (2007).
- [37] M. E. Möbius, G. Katgert, and M. van Hecke, *Europhys. Lett.* **90**, 44003 (2010).
- [38] G. Picard, A. Ajdari, F. Lequeux, and L. Bocquet, *Eur. Phys. J. E* **15**, 371 (2004).
- [39] J. Chattoraj, C. Caroli, and A. Lemaître, *Phys. Rev. E* **84**, 011501 (2011).
- [40] P. Chaudhuri, L. Berthier, and W. Kob, *Phys. Rev. Lett.* **99**, 060604 (2007).
- [41] J. D. Weeks, D. Chandler, and H. C. Andersen, *J. Chem. Phys.* **54**, 5237 (1971).
- [42] D. J. Durian, *Phys. Rev. Lett.* **75**, 4780 (1995).
- [43] H. J. Hwang, R. A. Riggleman, and J. C. Crocker, *Nat. Mater.* **15**, 1031 (2016).
- [44] J. M. Brader, M. E. Cates, and M. Fuchs, *Phys. Rev. Lett.* **101**, 138301 (2008).
- [45] N. D. Denkov, S. Tcholakova, K. Golemanov, K. P. Ananthapadmanabhan, and A. Lips, *Soft Matter* **5**, 3389 (2009).
- [46] O. I. Vinogradova, K. Koynov, A. Best, and F. Feuillebois, *Phys. Rev. Lett.* **102**, 118302 (2009).
- [47] C. Donati, J. F. Douglas, W. Kob, S. J. Plimpton, P. H. Poole, and S. C. Glotzer, *Phys. Rev. Lett.* **80**, 2338 (1998).
- [48] A. Stukowski, *Model. Simul. Mater. Sci. Eng.* **18**, 015012 (2010).
- [49] M. L. Falk and J. S. Langer, *Phys. Rev. E* **57**, 7192 (1998).
- [50] V. Chikkadi and P. Schall, *Phys. Rev. E* **85**, 031402 (2012).
- [51] J.-P. Bouchaud, S. Gualdi, M. Tarzia, and F. Zamponi, *Soft Matter* **12**, 1230 (2016).
- [52] M. Bouzid, M. Trulsson, P. Claudin, E. Clément, and B. Andreotti, *Phys. Rev. Lett.* **111**, 238301 (2013).
- [53] D. Bonn, M. M. Denn, L. Berthier, T. Divoux, and S. Manneville, *Rev. Mod. Phys.* **89**, 035005 (2017).